Journal Pre-proof

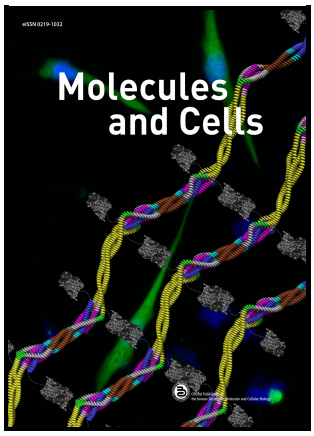

A comparison study of pathological features and drug efficacy between *Drosophila* models of C9orf72 ALS/FTDRunning title: A comparative analysis on G_4C_2 models

Davin Lee, Hae Chan Jeong, Seung Yeol Kim, Jin Yong Chung, Seok Hwan Cho, Kyoung Ah Kim, Jae Ho Cho, Byung Su Ko, In Jun Cha, Chang Geon Chung, Eun Seon Kim, Sung Bae Lee

PII: S1016-8478(23)25255-3

DOI: https://doi.org/10.1016/j.mocell.2023.12.003

Reference: MOCELL5

To appear in: *Molecules and Cells*

Received date: 28 July 2023
Revised date: 11 November 2023
Accepted date: 13 November 2023

Please cite this article as: Davin Lee, Hae Chan Jeong, Seung Yeol Kim, Jin Yong Chung, Seok Hwan Cho, Kyoung Ah Kim, Jae Ho Cho, Byung Su Ko, In Jun Cha, Chang Geon Chung, Eun Seon Kim and Sung Bae Lee, A comparison study of pathological features and drug efficacy between *Drosophila* models of C9orf72 ALS/FTDRunning title: A comparative analysis on G_4C_2 models, *Molecules and Cells,* (2023) doi:https://doi.org/10.1016/j.mocell.2023.12.003

MOLCELLS-2023-0120

Received 28-Jul-2023

revised 11-Nov-2023

accepted 13-Nov-2023

https://doi.org/10.14348/molcells.2024.2120

A comparison study of pathological features and drug efficacy between *Drosophila* models of C9orf72 ALS/FTD

Davin Lee[1,5], Hae Chan Jeong[1,5], Seung Yeol Kim[2], Jin Yong Chung[2], Seok Hwan Cho[2], Kyoung Ah Kim[1], Jae Ho Cho[1], Byung Su Ko[1], In Jun Cha[3], Chang Geon Chung[4], Eun Seon Kim[1,*], Sung Bae Lee[1,*]

[1]Department of Brain Sciences, Daegu Gyeongbuk Institute of Science and Technology (DGIST), Daegu 42988, Republic of Korea

[2]SK Biopharmaceuticals Co., Ltd., Seongnam 13494, Republic of Korea

[3]Brain Research Policy Center, Korea Brain Research Institute, Daegu 41068, Republic of Korea

[4]Department of Neurology, Johns Hopkins University School of Medicine, Baltimore, Maryland 21205, USA

[5]These authors contributed equally to this work.

*Correspondence to: eunseon_k@dgist.ac.kr; sblee@dgist.ac.kr

Keyword: Comparison study, G_4C_2 repeat expansion models, *C9orf72*, ALS, drug screening

Running title: A comparative analysis on G_4C_2 models

ABSTRACT

Amyotrophic lateral sclerosis (ALS) is a devastating neurodegenerative disease with a complex genetic basis, presenting both in familial and sporadic forms. The hexanucleotide (G_4C_2) repeat expansion in the *C9orf72* gene, which triggers distinct

pathogenic mechanisms, has been identified as a major contributor to familial and sporadic ALS cases. Animal models have proven pivotal in understanding these mechanisms; however, discrepancies between models due to variable transgene sequence, expression levels, and toxicity profiles complicate the translation of findings. Herein, we provide a systematic comparison of seven publicly available *Drosophila* transgenes modeling the G_4C_2 expansion under uniform conditions, evaluating variations in their toxicity profiles. Further, we tested three previously characterized disease modifying drugs in selected lines to uncover discrepancies among the tested strains. Our study not only deepens our understanding of the *C9orf72* G_4C_2 mutations but also presents a framework for comparing constructs with minute structural differences. This work may be used to inform experimental designs to better model disease mechanisms and help guide the development of targeted interventions for neurodegenerative diseases, thus bridging the gap between model-based research and therapeutic application.

INTRODUCTION

Amyotrophic lateral sclerosis (ALS) is a progressive neurodegenerative disorder that primarily affects motor neurons in the brain and spinal cord, resulting in muscle weakness, paralysis and eventual death (DeJesus-Hernandez et al., 2011). Central to ongoing research efforts is the determination to better comprehend the genetic contributors of ALS (Byrne et al., 2013; Kwiatkowski et al., 2009; Rosen et al., 1993; Shatunov et al., 2010). Although only 5-10% of ALS cases are familial (Majounie et al., 2012), a significant percentage of sporadic cases also present genetic cause (Van Daele et al., 2023), prompting extensive inquiries into unraveling the genetic underpinnings and complex pathogenesis of ALS.

One of the major breakthroughs in ALS research is the identification of the hexanucleotide (G_4C_2) repeat expansion in the *C9orf72* gene, which accounts for the largest proportion of familial ALS cases (DeJesus-Hernandez et al., 2011). The expansion results in reduced expression of the *C9orf72* gene (Shi et al., 2018) as well as the formation of RNA foci, which are accumulations of transcribed repeat RNA (Zu et al., 2013). These RNA foci are found to sequester RNA-binding proteins and disrupt RNA processing and splicing (Lee et al., 2013). Furthermore, the transcribed RNA from the G_4C_2 expansion forms stable G-quadruplex structures, which may modulate translation frequency (Conlon et al., 2016). Interestingly, the repeat expansion triggers an unusual repeat-associated non-AUG (RAN) translation, producing dipeptide repeat (DPR) proteins that are prone to aggregation and toxic to various cellular components (Ash et al., 2013). Notably, this same mutation is also observed in frontotemporal dementia (FTD) (Ash et al., 2013; Devenney et al., 2014), suggesting that advancements made in G_4C_2 pathogenesis could have broader implications for understanding and treating both ALS and FTD.

Given the complex characteristics of the G_4C_2 repeat expansion in the *C9orf72* gene, numerous animal models have been generated to accurately represent the disease (Batra & Lee, 2017). In fact, animal models expressing disease-associated transgenes

have been instrumental in elucidating the complexities of G_4C_2-mediated disease pathogenesis. These models enabled us to study how ALS or other G_4C_2-associated neurodegenerative diseases progress *in vivo* and discover potential therapeutic interventions. However, these transgenic animal models are not without limitations.

In many animal models, transgenes are usually overexpressed to a nonphysiological level due to the usage of strong promoters and the absence of regulatory sequences that are normally present in the untranslated regions (UTRs). This can lead to exaggerated phenotypical results, creating disparities between animal models and human disease. Importantly, minute differences in the transgene configuration can have consequential effects on the observed disease phenotype. For example, while most G_4C_2 transgene constructs use uninterrupted pure G_4C_2 repeats, the $(G_4C_2)_{44}$ construct includes an intronic 5' leader sequence (LDS), an attempt to more closely mimic the genetic configuration observed in ALS patients, leading to notable differences in DPR expression and toxicity (Goodman, Prudencio, Srinivasan, et al., 2019; Kearse et al., 2016). This diversity, while valuable for studying specific aspects of the disease, complicates the comparison and interpretation of results across studies. Further confounding the issue is the variability in toxic profiles, such as the expression of DPR(s), across models, which makes it difficult to delineate the relative contributions of each pathogenic mechanism and identify potential therapeutic targets.

Therefore, it is imperative to undertake an unbiased and systematic comparison of available transgenes of G_4C_2, assessing the toxic profiles and variations in transgene constructs. This endeavor not only enhances our understanding of C9orf72-G_4C_2 mutations but also establishes a framework for assessing constructs with minute structural differences that can have significant consequences. Such a framework is essential for informing experimental designs that accurately model disease mechanisms and for guiding the development of targeted therapeutic interventions. In this article, we contribute to this vital area by providing a comparative analysis of seven publicly available *Drosophila* transgenes that model the G_4C_2 expansion. We also establish a framework wherein we conducted phenotype testing under uniform conditions, ensuring that the transgenes are subjected to comparable environments, thereby enabling a more precise and controlled analysis of their toxicity profiles. Through our analysis, we aim to offer insights into the molecular consequences of variations in transgene constructs, and underscore the nuances that should be considered in future studies involving G_4C_2 expansion modeling. Ultimately, these comparative analyses and the framework developed may help underpin a more comprehensive understanding of the molecular mechanisms at play, which is fundamental for the advancement of targeted strategies in the management and treatment of neurodegenerative diseases.

MATERIALS AND METHODS

Drosophila stocks

All flies were maintained at 27°C and 25% humidity. The following lines were obtained from Bloomington *Drosophila* Stock Center (USA): *Elav-Gal4* (8765), *GMR-Gal4*

(1104), *UAS-luciferase* (35788), *UAS-$(G_4C_2)_{36}$* (58688), *UAS-LDS-$(G_4C_2)_{44}$.GR-GFP/TM3* (84723), *UAS-$(G_4C_2)_{49}$/TM6C* (84726), *UAS-$(G_4C_2)_{49}$* (84727). Using a transposon-based approach, the *GMR-Gal4* (III) was generated by relocating transgene from its original position on the 2nd chromosome to the 3rd chromosome. *UAS-$(G_4C_2)_{30}$/cyo* and *UAS-$(G_4C_2)_{30}$/Tm3* were provided by Peng Jin (Emory University, USA). *UAS-$(G_4C_2)_{160}$* line was provided by Fen-Biao Gao (University of Massachusetts, USA).

Molecular cloning and generation of transgenic flies

UAS-HA-Rhau was synthesized and subcloned into pACU2 vectors using NOTI and XbaI, and the HA epitope was added at the N-terminus. Transgenic flies were generated by BestGene, Inc. Nucleotide sequences are available upon request.

Immunohistochemistry (IHC) for fly brain

As previously described by Park et al. (Cho et al., 2022; Park et al., 2020; Ryu et al., 2022), adult flies were dissected in Schneider's insect medium (Cat No. S0146; Sigma, USA) to obtain brain samples for immunohistochemical analysis. Brains were fixed with 3.7% formaldehyde for 20 min at room temperature. After washing with PBST (0.3% Triton-X100 in phosphate-buffered saline), brains were incubated in a blocking buffer (5% Normal donkey serum in 0.3% PBST) for 1 h at room temperature (RT). Next, the brains were incubated in the primary antibody overnight at 4°C. The following primary antibodies were used in this study: α-GP rabbit (proteintech, 24494-I-AP) at 1:200 concentration, α-rRNA(Y10b) mouse (NOVUS, NB100-662) at 1:200 concentration, α-dTDP-Gly rabbit (gift by James Shen at Taipei Medical University) at 1:200 concentration. Brains were then washed with washing buffer three times for 10 min each. Then, brains were further incubated in the secondary antibody for 2 h at room temperature. The following secondary antibodies were used: α-rb alexa555 (Thermo Fisher Scientific, Z25305) at 1:200 concentration, α-rb alexa647 (Invitrogen, A21244) at 1:200 concentration, α-mouse alexa647 (Invitrogen, A21236) at 1:200 concentration, α-rb alexa488 (Abcam, A11034) at 1:200 concentration. Brains were washed five times with washing buffer prior to mounting on a slide glass for imaging. DAPI was used as a mounting medium. The posterior regions of mushroom body Kenyon cells were used for DPR analysis.

Protein extraction and western blotting

Total protein extraction and Western blot analysis was performed as previously described with minor modification (Park et al., 2020). 30 adult fly heads were suspended in lysis buffer (50 mM Tris-buffered saline (Tris–HCL) pH 7.5, 150 mM NaCl, 1% Triton ×100) containing protease inhibitor cocktail (Thermo Scientific, #87786; 1:100) and homogenized. 30 μg of lysate was mixed with Laemmli buffer (Bio-Rad, #161-0747) to β -mercaptoethanol (BIOSESANG, #60-24-2) and boiled at 95°C for 5 min. The lysates were loaded on 10% SDS-PAGE gel for 2 hours at 70 V and then transferred to the nitrocellulose membrane (Bio-Rad, BR170-4270) for 1 hour at 100 V. The membrane was incubated in blocking buffer [1X TBS (BIO-RAD, #1706435), 0.1 % Tween-20, and 5% skim milk] for 1 hour at room temperature (RT). Primary antibodies were used as follows: mouse anti-MAP Kinase (Sigma, M8159, 1:1000), rabbit anti-P-SAPK/JNK (Cell signaling, #4668S, 1:1000), rabbit anti-GRP78 (BiP) antibody (StressMarq Biosciences, SPC-180); and mouse anti-alpha tubulin (DSHB, E7-s, 1:2000). The secondary antibodies were used: goat anti-mouse-IgGκ BP-HRP

(santa cruz, sc-516102, 1:2000); and goat anti-rabbit IgG, F(ab')2-HRP (santa cruz, sc-3837, 1:2000). Lumigen ECL Ultra (Lumigen, TMA-6) was treated prior to detection at ChemiDoc™ XRS+.

RNA extraction and quantitative real-time RT-PCR (qRT-PCR)

RNA extraction and cDNA synthesis of fly samples were performed as previously described (Chung et al., 2017; Lee et al., 2023; Lee et al., 2022). Total RNAs were extracted from adult fly heads or adult whole bodies using Easy-Blue system (iNtRON Biotechnology). cDNAs were synthesized from 3 μg of total RNAs using GoScript Reverse Transcription (Promega, A2791) according to the manufacturer's standard protocol. Quantitative PCR (qPCR) experiments were performed using the synthesized cDNAs with QuantiSpeed SYBR Green kit (PhilKorea, QS105-10) and CFX96 TouchTM Real-Time PCR Detection System (Bio-Rad). Gene specific primers were listed in Supplementary Figure S5a (Tran et al., 2015; Xu et al., 2013). rp49 was used as a housekeeping gene when analyzing fly samples. mRNA fold change of each gene was calculated using the comparative Ct method. Gene-specific primers were designed with Primer-BLAST (ncbi.nlm.nih.gov/tools/primer-blast) and *Drosophila* RNAi Screening Center (DRSC) FlyPrimerBank (flyrnai.org/flyprimerbank). Some primer sequences were obtained from published studies.

Conditions for acquiring and imaging eye phenotypes

Depending on the data, eye images of 1d, 7d or 10d adult flies expressing G_4C_2 repeats under the control of *GMR-Gal4* at 25°C or 27°C and 25% humidity were acquired with a Nikon Eclips 90i.

Negative geotaxis assay

Right after eclosion from pupa, 15 flies of each genotype were collected and reared for, depending on the experiment, 3d or 10d at 27°C with 25% humidity. After the assigned days, these flies were transferred to an acrylic cylinder closed at one end (3-cm diameter, 18-cm height) without CO_2 anesthesia, while the top of the cylinder was sealed with sponges to block escape. After 20min acclimation at room temperature, the flies were placed on the bottom of the cylinder by tapping the cylinder against a table, and climbing was recorded for 1 min. Climbing ability was measured with a climbing index (proportion of 15 flies climbing >10 cm from the bottom of cylinder within 10 s) in each experimental group of flies.

Lifespan assay

Lifespan assay were performed with guidance from a previous study (Pradhan et al., 2023). In each experiment, at least 100 male flies of each genotype were collected within 24 h after pupal eclosion (APE). Flies were maintained at low density (15 males per wide vial) at 27°C on a 12-hr light/12-hr dark cycle and transferred to new vials every 2 days. At each transfer, the number of dead flies was counted. Lifespan results are shown as Kaplan-Meier survival curves. Statistical differences were assessed with the log-rank test.

Image acquisition and processing

All IHC samples were taken at 400x magnification using 40x water immersion objective, acquired by Zeiss LSM780 confocal microscopy (Zeiss, Germany) at 20°C. Kenyon cells in the fly brains were taken to detect DPRs' expression. After image acquisition,

maximum-intensity projections of each image were obtained using Zeiss Zen software, and additional image processing (pseudo-color filters or deconvolution) was applied in Adobe Photoshop CC. The posterior regions of mushroom body Kenyon cells were imaged with uniform conditions and the pixel intensity was taken using histogram analysis.

Statistical analyses

Statistical analysis was done using GraphPad Prism 7 (GraphPad Software, USA). Depending on the data, we applied Student's t-test, Log-rank(Mantel-Cox) test or one-way ANOVA followed by Tukey's post-hoc analysis. In all figures, n.s., *, **, ***, and **** represent $P > 0.05$, $P < 0.05$, $P < 0.01$, $P < 0.001$, and $P < 0.0001$, respectively. Error bars are SEM.

RESULTS

Characteristics of G_4C_2 constructs used in the study

Table 1. Characteristics of G_4C_2 constructs used in the study. For each line, the transgene information, distinguishing features, the presence of AUG codons, the chromosome in which the construct is inserted, the presence of RNA foci (literature based), the presence of dipeptide repeat (DPR) proteins (literature based), the observation of toxicity (literature based), and relevant references are provided.

Identification		Transgene information			Reference-based toxicity			
BL number	**Transgene**	**Repeats**	**Distinguishing features**	**AUG codon**	**Inserted chromosome**	**RNA foci**	**DPR**	**Phenotype(s)**	**Reference(s)**
na	***(G_4C_2)$_{160}$***	160 repeats	Intronic 160 G_4C_2 repeat minigenes flanked by human intronic and exonic sequences	None	Chr 2.	Found (Tran et al., 2015)	Found GP (Tran et al., 2015)	Modest life-span toxicity at 29°C (Tran et al., 2015)	(Tran et al., 2015), (Yuva-Aydemir et al., 2019)
na	***(G_4C_2)$_{30}$*** **(III)**	30 repeats	Uninterrupted pure repeats	None	Chr 3.	n.a	n.a	Locomotion defects Eye degeneration (d14) (Xu et al., 2013)	(Xu et al., 2013), (Dubey et al., 2022)
na	***(G_4C_2)$_{30}$*** **(II)**			None	Chr 2.			Eye degeneration (d15) (Dubey et al., 2022)	
58688	***(G_4C_2)$_{36}$***	36 repeats	Uninterrupted pure repeats	None	Chr 2, 25C6, 2L:5108448.	Found (Mizielinska et al., 2014)	Found GR (Mizielinska et al., 2014)	Eye degeneration, Life-span, Egg-to-Adult viability (Mizielinska et al., 2014) [**strongly suggest the role of DPR toxicity]	(Mizielinska et al., 2014)

84723	***LDS-(G_4C_2)$_{44}$***	44 repeats	5′ leader sequence (LDS) inserted immediately upstream of the G_4C_2 repeats, 114 bp of sequence upstream of the repeat in intron 1 of *C9orf72* in patients, and a 3′ GFP tag in the GR reading frame.	None	Chr 3.	n.a	GFP-tagged GR	Eye degeneration (d15) (Cunningham et al., 2020) [*potential RNA toxicity involvement]	(Goodman, Prudencio, Srinivasan, et al., 2019), (Cunningham et al., 2020)
84726	***(G_4C_2)$_{49}$*** (III)	49 repeats	Uninterrupted pure repeats	None	Chr 3.	Found (Kramer et al., 2016)	Found GP (Kramer et al., 2016)	Eye degeneration, Life-span (Kramer et al., 2016)	(Goodman, Prudencio, Kramer, et al., 2019), (Kramer et al., 2016)
84727	***(G_4C_2)$_{49}$*** (II)			None	Chr 2.				

Comparative analysis of the neurotoxicity and pathological effects of various G_4C_2 constructs in *Drosophila* models

To evaluate the respective toxicities and pathologies of publicly available G_4C_2 constructs (Table 1. and Supplementary Figure S1a), we performed an in-depth comparative analysis in *Drosophila* using two different GAL4 drivers: *Elav-Gal4* and *GMR-Gal4*. Initially, we employed the *GMR-Gal4* driver to express the G_4C_2 constructs in the *Drosophila* eye, a well-established model for studying neurodegeneration. Using the degeneration severity criteria detailed in Supplementary Figure S1b, degeneration scores revealed that two lines had significantly higher scores compared to the other constructs (Figures 1a and 1b). While most G_4C_2 constructs, apart from $(G_4C_2)_{160}$, generated significant degenerative eye phenotypes, flies expressing $(G_4C_2)_{30}$ (II) and $(G_4C_2)_{36}$ demonstrated the most pronounced degeneration. Note that two $(G_4C_2)_{49}$ lines were excluded from the experiment due to their lethality when expressed in neurons or the eye at 27°C, thereby precluding further analysis.

Subsequently, we examined the climbing ability of the flies expressing different G_4C_2 constructs neuronally with the *Elav-Gal4* driver on days 3 and 10 to assess the progression of motor behavior impairments over time. As pan-neuronal expression of $(G_4C_2)_{30}$ transgenes using *Elav-Gal4* (I) caused developmental lethality (Xu et al., 2013), we used the *Elav-Gal4* (II) driver, a previously described non-lethal *Elav-Gal4* alternative (Wen et al., 2020), for our investigations. On day 3, both $(G_4C_2)_{30}$ lines demonstrated substantial toxicity, significantly impairing the climbing ability of the flies (Figure 1c). By day 10, the *LDS-*$(G_4C_2)_{44}$ line was the most affected among the flies that survived until adulthood, showing the steepest decline in motor function over time among flies observed (Figure 1d).

Finally, we assessed the lifespan of the flies expressing these constructs for a period of up to 30 days to measure the overall organismal health, complementing the relative short-term phenotypic effects observed in the eye and motor behavior assays. This revealed significant variations in the lifespan, with different constructs displaying differing levels of toxicity (Figure 1e). Importantly, the *LDS-*$(G_4C_2)_{44}$ line was found to be the most toxic, evidenced by the shortest lifespan among all the constructs studied. Additionally, the $(G_4C_2)_{36}$ construct showed a moderate effect on lifespan when expressed in neurons using *Elav-Gal4*.

Our results illustrate that the expression of G_4C_2 repeat expansion constructs in *Drosophila* leads to notable neurotoxic effects, with varying levels of toxicity among different constructs. Particularly, the *LDS-$(G_4C_2)_{44}$* line was highly toxic, exhibiting detrimental effects on both climbing and lifespan phenotypes, while demonstrating a milder phenotype in eye degeneration. Moreover, the *$(G_4C_2)_{30}$* (II) line was highly toxic in the climbing assay and eye degeneration, indicating impaired neuronal function, while the *$(G_4C_2)_{36}$* showed consistent moderate toxicity in performed assays. These findings elucidate the neurotoxic impact of G_4C_2 repeat expansion constructs in *Drosophila*, highlighting the varying degrees of toxicity among different constructs.

Detection of GP DPRs and TBPH in the brains of G_4C_2-expressing *Drosophila*

We found that the expression of seven publicly available G_4C_2 repeat transgenes resulted in differing degrees of toxicity. Existing literature indicates a strong correlation between DPRs and neuronal toxicity (Lee et al., 2016; Mizielinska et al., 2014), which led us to hypothesize that elevated concentrations of DPR proteins could be observed in flies exhibiting the highest behavioral or cellular degeneration.

To test this hypothesis, we utilized a well-established DPR antibody specific to poly-glycine-proline (GP) repeats (Dafinca et al., 2016) as a representative DPR marker and observed its expression in the *Drosophila* CNS. In line with our hypothesis, we observed considerable GP DPRs in both *$(G_4C_2)_{30}$* (II) and *LDS-$(G_4C_2)_{44}$* expressing fly lines, whereas other lines exhibited relatively low GP DPR expression levels (Figure 2a and 2b). Surprisingly, despite showing moderate phenotypic toxicity, the fly brains expressing *$(G_4C_2)_{36}$* showed little-to-no evidence of GP DPR expression, possibly suggesting involvement of other toxic DPRs, such as GR DPR (Mizielinska et al., 2014). Interestingly, the GP DPRs largely lacked the co-localization with DAPI staining, suggesting that GP DPRs, similar with previous findings (Goodman, Prudencio, Srinivasan, et al., 2019), were expressed in the cytoplasm of Kenyon cells. In addition, to validate that signals from GP staining can be used as a representative marker for DPRs, we utilized the *LDS-$(G_4C_2)_{44}$* transgene and tracked the localization of GR DPR by detecting green fluorescent protein (GFP) signals in the brain. While significant GR expression was, as expected, observed, the GFP signals were predominantly in the Kenyon cell nucleus, contrary to the GP DPRs (Supplementary Figure S2a). This suggests that DPR proteins predominantly localize in distinct subcellular localizations, as previously indicated by Wen et al (Wen et al., 2014).

In our investigation into the pathological markers associated with G_4C_2 repeats expansion, we turned our attention to the mislocalization of TDP-43 (TBPH) in *Drosophila*, a phenomenon well-documented in various neurodegenerative disorders as well as C9orf72 repeat-associated expansion (Haeusler et al., 2016; Park et al., 2020; Solomon et al., 2018). Utilizing a previously used TBPH-specific antibody (Lin et al., 2011; Park et al., 2020), we analyzed the localization patterns of this protein across our fly models within the Kenyon cells. Our observations revealed a shift in TBPH localization under the influence of G_4C_2 expression (Supplementary Figure S2b). Contrary to the predominant nuclear presence of TBPH in control cells, models

expressing G_4C_2 exhibited a discernible decrease in nucleus TBPH while an increase in cytoplasmic TBPH inclusion, indicating a potential involvement of alterations in the nuclear-cytoplasmic transport mechanisms, a finding that aligns with current scientific discourse on neurodegenerative pathologies (Gasset-Rosa et al., 2019; Park et al., 2020; Solomon et al., 2018).

Due to previous reports indicating that repeat-associated RNA toxicity may be involved in cellular or behavioral defects (Cunningham et al., 2020; Goodman, Prudencio, Srinivasan, et al., 2019; Kim et al., 2021; McEachin et al., 2020), we quantified the transgene-specific RNA levels in various transgene expressions through quantitative reverse transcription PCR (qRT-PCR) analysis (Supplementary Figure S5a-d). Our findings demonstrated a marked increase in RNA transgenes across all measured fly lines, with specific RNA measures correlating with our earlier toxicity profiles (Figure 1a-e). This correlation, however, should be approached with a degree of caution due to the methodological challenges in comparing RNA levels across different transgenes (see discussion).

Collectively, these results not only support the notion that DPRs, such as GP and GR DPRs, exhibit distinct subcellular localizations and potentially possess varying mechanisms of action but also highlight the consistency of our data with findings from other literature underscoring the reliability of our platform to model G_4C_2-related diseases. Future research is essential to delve deeper into these mechanisms and to investigate possible therapeutic strategies to counter G_4C_2-related neurotoxicity.

Evaluating drug efficacy against G_4C_2 toxicity: Impacts on lifespan, mobility, and eye degeneration in *Drosophila* models

In the present investigation, our attention was concentrated primarily on the *LDS-$(G_4C_2)_{44}$* and *$(G_4C_2)_{30}$* (II) transgene constructs. This choice was guided by several factors. Primarily, these models displayed high toxicity levels in the three preceding tests (eye degeneration analysis, climbing ability analysis, and lifespan analysis) without reaching lethality, a critical attribute for deriving measurable results. Constructs such as *$(G_4C_2)_{49}$* were eliminated from consideration due to their extreme toxicity levels, which led to lethality and thereby precluded further analysis. Conversely, constructs that exhibited weak to mere moderate toxicity lacked the sensitivity and robustness required for a valuable model to evaluate the potential therapeutic interventions. Similarly, we selected constructs that demonstrated DPR expression, intrigued to investigate potential alterations in DPR expression or localization induced by our therapeutic agents.

We next sought to investigate the potential of specific therapeutic candidates in mitigating these effects (Supplementary Figure S3a). As such, we chose three compounds, TMPyP4, PJ34, and KPT-276, for evaluation due to their distinct mechanisms of action in relation to different stages of G_4C_2 toxicity. TMPyP4 is known to bind to and destabilize G-quadruplexes, potentially affecting the stability of G_4C_2 repeats and thereby reducing both RNA and protein toxicity (Zamiri et al., 2014). PJ34

is an inhibitor of poly (ADP-ribose) polymerase and is specifically considered for attenuating protein toxicity (Gao et al., 2022). KPT-276 inhibits the nuclear export of proteins and RNA, and thus might affect G_4C_2-related pathologies through modulating nucleocytoplasmic trafficking (Chou et al., 2018; Schmidt et al., 2013). This selection of drugs allowed us to target and dissect various aspects of G_4C_2 toxicity.

We first assessed the impact of TMPyP4, PJ34, and KPT-276 on the lifespan of flies expressing the *LDS-*$(G_4C_2)_{44}$ line using *Elav-Gal4* (Figures 3a, 3b, Supplementary Figure S3b). The dosages administered were based on established concentrations from prior studies using the *Drosophila* ALS models, ensuring methodological consistency and comparability of our results with existing literature (Chou et al., 2018; Gao et al., 2022; Schmidt et al., 2013; Zamiri et al., 2014). Both TMPyP4 and PJ34 treatments significantly extended the lifespan of these flies compared to controls. However, KPT-276 did not exhibit a notable effect on lifespan (Supplementary Figure S3b).

Next, we investigated the effects of three above-mentioned drugs on the climbing ability of flies expressing the $(G_4C_2)_{30}$ (II) and *LDS-*$(G_4C_2)_{44}$ lines (Figures 3c, 3d, Supplementary Figure S3c). We observed that TMPyP4 and PJ34 had beneficial effects on the climbing ability, but only in the $(G_4C_2)_{30}$ (II) expressing flies. No significant improvement in the climbing ability of the *LDS-*$(G_4C_2)_{44}$ line was seen. KPT-276 did not affect the climbing ability of flies expressing the two G_4C_2 transgenes (Supplementary Figure S3c).

Lastly, we used *GMR-Gal4* to express $(G_4C_2)_{30}$ (II) and *LDS-*$(G_4C_2)_{44}$ in the eyes of flies and evaluated the effects of TMPyP4, PJ34, and KPT-276 on eye degeneration (Figures 3e-h, Supplementary Figure S3d, S3e) using the degeneration severity criteria detailed in Supplementary Figure S1b and S1c. Remarkably, all three drugs showed a beneficial effect in reducing the degeneration scores for both G_4C_2 constructs, indicating their potential in alleviating eye pathologies associated with G_4C_2 toxicity (with the exception of KPT-276, which alleviated the eye degeneration in $(G_4C_2)_{30}$ (II) but not *LDS-*$(G_4C_2)_{44}$).

Our results indicate that TMPyP4 ameliorates disease phenotype, reinforcing the notion that destabilizing RNA G_4C_2 G-quadruplex structures can inhibit associated toxicity (Li et al., 2021; Mishra et al., 2019). Recent studies have unveiled that an RNA helicase, *DHX36*, can modulate the toxicity of G_4C_2 by acting on repeat RNA G-quadruplexes and facilitating RAN translation (Liu et al., 2021; Tseng et al., 2021). Given these findings, we were interested to explore whether genetic modulation of G-quadruplex regulators can affect disease phenotype in our experimental platform. To address this, we generated transgene RNA helicase associated with AU-rich element (Rhau), the *Drosophila* homologue of *DHX36* and a potent G-quadruplex unwinder, and co-expressed it with $(G_4C_2)_{30}$ (II) and observed the *Drosophila* eye degeneration intensity. Our results confirm that the co-expression of *Rhau* with $(G_4C_2)_{30}$ (II) did in fact amplify the toxicity, suggesting a role for *Rhau* in exacerbating the disease phenotype (Supplementary Figure S3f, S3g), a finding consistent with previous literatures (Liu et al., 2021; Tseng et al., 2021). These results imply that our platform

may be applied not only for the testing of pharmacological drugs but also for exploring genetic modulations.

Our data indicate that TMPyP4 and PJ34 can ameliorate some of the toxic effects associated with G_4C_2 constructs, particularly in extending lifespan and improving climbing ability in specific constructs. Moreover, TMPyP4, PJ34, and KPT-276 were all effective in reducing eye degeneration associated with G_4C_2 toxicity. These findings provide valuable insights into potential therapeutic strategies for conditions associated with G_4C_2 repeat expansions and underscore the importance of targeting different aspects of G_4C_2 toxicity.

Impact of representative G_4C_2-associated drugs on GP DPR in *Drosophila* models

Given that the three previously characterized disease modifying drugs - TMPyP4, PJ34, and KPT-276 – were able to elicit amelioration of G_4C_2-associated toxicity in *$(G_4C_2)_{30}$* (II) and *LDS-$(G_4C_2)_{44}$* expressing flies, we decided to investigate the expression and localization of DPR proteins. We hypothesized that the beneficial effects observed in Figure 3 could potentially result from a change in the localization of -, or the reduction of DPR proteins.

In accordance with this hypothesis, we found that treatment with TMPyP4 at 100μM led to a reduction in DPR expression in both *$(G_4C_2)_{30}$* (II) and *LDS-$(G_4C_2)_{44}$* lines (Figure 4a and 4c). TMPyP4 is a known G-quadruplex destabilizer, and its ability to reduce the expression of DPR proteins suggests that it may be acting through destabilization of the G-quadruplex structures in the G_4C_2 region, thereby inhibiting the aberrant translation process that generates the toxic DPRs (Wang et al., 2019). Similarly, treatment with PJ34 also led to a decrease in GP signals but only in *LDS-$(G_4C_2)_{44}$* lines (Figure 4b and 4d). However, PJ34's effects were not as potent as TMPyP4's and both were no observable changes in the localization of GP proteins. Interestingly, KPT-276, a selective nuclear export inhibitor, fed flies showed no difference in GP signals in comparison to the control group (Supplementary Figure S4a and S4b). It is important to note that all three drugs were unable to significantly reduce (or alter the localization of-; data not shown) GR DPRs, as measured by GFP signals in *LDS-$(G_4C_2)_{44}$* lines (Supplementary Figure S4c-f).

Taken together, these data provide evidence that TMPyP4, PJ34, can reduce or ameliorate the toxic effects of G_4C_2 transgenes. Because our study primarily concentrates on the reduction of GP, a commonly recognized non-toxic DPR, it is crucial to extend research to include the distribution of other DPR proteins, such as GA, PR, or even chimeric DPRs. In addition, it remains inconclusive whether these drugs can reduce GR DPRs in other flies expressing transgenes other than *LDS-$(G_4C_2)_{44}$*. This exploration would provide a firmer understanding of the effects of the three-representative disease-modifying drugs.

DISCUSSION

In this study, we utilized available *Drosophila* transgenic models of C9orf72-G_4C_2 mutations for a comprehensive and unbiased examination of the neurotoxic and pathological consequences. Our systematic comparative analysis indicates that these constructs are associated with distinct toxicity profiles, which encompass degenerative effects on the eye, impairment of climbing ability, and a reduction in lifespan, thereby suggesting a well-substantiated model for the exploration of neurodegeneration. Moreover, we present an experimental framework that aids in comprehending how factors, such as subtle sequential differences, may engender significant disparities in both toxicity profiles and drug treatment outcome (Figure 5). Although it remains elusive which specific constructs are responsible for higher G_4C_2 expression levels, their differential expression patterns warrant investigation to elucidate the reasons behind variable toxicities among constructs. This knowledge may be pivotal in shaping future research directions.

In addition to DPR toxicity, RNA toxicity may play a role in neurodegeneration. To test this hypothesis, we performed qRT-PCR using construct-specific primers to quantify G_4C_2 RNA levels (Supplementary Figure S5a-d) within the same category of G_4C_2 transgenes. We found that all tested transgenes showed significant increase in probed RNA. Interestingly, we found that the *$(G_4C_2)_{30}$* (II) line exhibited higher RNA levels compared to *$(G_4C_2)_{30}$* (III) line, consistent with our toxicity profile data (Supplementary Figure S5c). However, interpreting these RNA results necessitates caution, primarily since a direct quantitative comparison of RNA across different transgenes is methodologically constrained due to inherent variations in used primers for qRT-PCR. These findings suggest the need for further comprehensive studies to delineate the potential toxicity caused by RNA in the context of G_4C_2 expansions and neurodegeneration. Nonetheless, the successful conduction of qRT-PCR using different primers offers promising prospects for advancing our understanding of this complex area of research.

Since all fly brains expressing G_4C_2 repeat-associated transgenes showed increased expression level of G_4C_2 RNA compared to control, we were curious to see whether aberrant G_4C_2 expression might precipitate global RNA irregularities. To examine this, we employed ribosomal RNA (rRNA) antibodies, which revealed a significant augmentation in cytoplasmic rRNA foci in both *$(G_4C_2)_{30}$* (II) and *LDS-$(G_4C_2)_{44}$* lines (Supplementary Figure S5e and S5f). This phenotype is particularly interesting in light of prior studies that have underscored that G_4C_2 expression contributes not just to TDP-43 aggregation but also leads to the formation of RNA foci in the cytoplasm. Nevertheless, we must tread carefully in interpreting the rRNA foci data, as the precise genesis of these structures remains undetermined, and their functional implications within cellular pathology are still to be unraveled. Future studies employing molecular investigations to elucidate the origins and consequential ramifications of rRNA foci formation in relation to G_4C_2 expression will be beneficial in understanding G_4C_2 repeat expansion-associated RNA toxicity.

Beyond the insights gained regarding G_4C_2 toxicity, our *Drosophila* platform

demonstrates a promising utility in therapeutic development. As well as providing an effective model for screening potential pharmacological interventions such as TMPyP4, PJ34, and KPT-276, this platform may also serve as a powerful tool for genetic interactor screenings, as exemplified by our findings from *Rhau* expression studies. Genetic screenings can offer critical insights into the molecular mechanisms underlying G_4C_2 toxicity and the pathology of associated diseases. They can identify genetic modifiers, potential risk factors, and potential therapeutic targets, by help pinpointing genes or genetic interactions that modulate the toxicity of G_4C_2 repeats. Hence, our platform could serve as a resource in the wider scientific community, not only for testing therapeutic efficacy but also for uncovering novel molecular pathways involved in G_4C_2-related pathologies.

The results from our study also shed light on the controversial efficacy of KPT-276. Recent studies have questioned the effectiveness of KPT-276 in improving quality-of-life in various diseases (Boeynaems et al., 2016; Lee et al., 2016). Our study corroborates these findings, as KPT-276 was found to be ineffective in extending the lifespan or improving the climbing ability of flies expressing *LDS-$(G_4C_2)_{44}$*. However, we observed a beneficial effect of KPT-276 in reducing eye degeneration in flies expressing the *$(G_4C_2)_{30}$* construct as depicted in a previous study (Zhang et al., 2015). This suggests that while KPT-276 may have a role in certain facets of G_4C_2 toxicity, its therapeutic potential may be limited or context-dependent (Vanneste & Van Den Bosch, 2021). These results lend additional credibility to our platform, demonstrating its capacity to reflect real-world clinical data, and thus reinforcing its reliability as a tool for drug efficacy evaluation.

Our study accentuates the necessity for strategic selection of G_4C_2 constructs in ALS research. Researchers would benefit from consideration of the particular aspect of toxicity or pathological feature they seek to investigate. For instance, a construct producing abundant DPRs would be more suitable for studies focusing on protein aggregation, whereas those forming G-quadruplexes might be apt for RNA toxicity studies. By strategically selecting G_4C_2 constructs, researchers can design experiments that more accurately model the specific disease mechanisms and evaluate the efficacy of targeted therapeutic interventions.

In addressing the variations observed in GP amounts between different G_4C_2 models, it is important to note crucial technical limitations of our study. Our primary evidence for comparing GP expression levels are the GP signal differences measured through IHC-based imaging techniques, which can be misleading in quantifying protein levels (Figure 2a and 2b). Therefore, we performed a western blot analysis using both GP- and GR-specific antibodies in fly brains expressing G_4C_2 repeat constructs to 1) validate the GP- and GR-specific antibodies used for IHC and 2) compare DPR protein quantities between different G_4C_2 models. While we were able to detect GP or GR in *LDS-$(G_4C_2)_{44}$* expressing flies that harbors a GFP tag in the GR repeat frame (or a single off-framed GFP in the GP repeat frame), thereby suggesting that the GP- and GR-specific antibodies are likely specific and effective, we were unable to detect measurable amount of GP or GR DPRs in other lines (data not shown). We speculate that the detection of DPRs in *LDS-$(G_4C_2)_{44}$* expressing flies may stem from the nature

of fused GFP, which resulted in increased size and stabilization of *LDS-$(G_4C_2)_{44}$*-derived GP or GR protein which made possible to overcome detection threshold of western blot analysis. Additionally, we speculate that the inability to detect GP or GR DPRs in other transgenes expressing flies may be due to the constitution of the G_4C_2 repeat constructs employed in our models. Aside from $(G_4C_2)_{160}$, the constructs used for western blotting analysis were of lengths no greater than 44 repeats, which are likely insufficient for the production of detectable levels of GP or GR proteins. Boivin et al., encountered similar challenges, reporting an inability to detect DPRs derived from very short G_4C_2 repeats, often less than 10 repeats, even when these sequences were tagged. They hypothesized that such minute DPR proteins likely possess inherent instability, resulting in rapid turnover, which significantly hinders their detectability in standard assay conditions (Boivin et al., 2020). It is also possible that conventionally used gels or membranes for Western blotting is insufficient in separating and retaining small proteins. This variability necessitates cautious interpretation of our results. Future studies aiming to quantify DPR levels will benefit from developing enhanced methodologies that can reliably detect and measure smaller or less stable DPR proteins, thereby providing a more comprehensive understanding of their role in ALS/FTD pathology.

It also remains unclear whether these differences in GP signal changes are due to variations in RAN translation efficiency or discrepancies in the transcription levels of the transgenes. It is important to acknowledge that the process of RNA translation is subject to a multitude of influencing factors, including, but not limited to, availability of ribosomes, the engagement of various initiation factors, specific configurations of mRNA secondary structures, interactions with diverse RNA-binding proteins, and a range of post-transcriptional modifications. Each of these elements can significantly impact the translation process, adding layers of complexity to our understanding of the observed phenomena. Such intricacies in the mechanisms governing RNA translation necessitate a more detailed investigative approach, incorporating advanced kinetics and comprehensive biochemical assays, to unravel the underlying causes of the observed differences in protein levels. Future studies should be conducted to delve deeper into these aspects, potentially utilizing advanced methodologies capable of dissecting the nuanced interplay of factors impacting RNA translation in the context of G_4C_2 repeat expansion.

Our investigation provides a framework for future studies into G_4C_2-associated ALS. Future directions should include evaluating the interplay between G-quadruplexes and DPRs in neuronal toxicity, and how these features can be modulated for therapeutic gains. There is a need for more comprehensive toxicity profiling of the candidate compounds in mammalian models of ALS, including pharmacokinetic and pharmacodynamic assessments. Additionally, the development of high-throughput screening assays utilizing the standardized *Drosophila* constructs could facilitate the identification of novel therapeutic candidates. In conclusion, while the *Drosophila* model offers promising insights and a platform for G_4C_2-associated ALS research, it is essential to acknowledge the complexities and heterogeneity of human pathology. The translation of these findings to human therapeutics, although potentially transformative,

necessitates careful and robust validation through in-depth molecular studies and comprehensive clinical trials.

ACKNOWLEDGEMENT

This work was supported by Basic Science Research Program through the National Research Foundation of Korea (2022R1A4A2000703 and 2021R1A2C1003817) and the Korea Brain Research Institute (KBRI) Research Program (23-BR-03-02), funded by the Ministry of Science and ICT, Republic of Korea and the Korea Health Technology R&D Project through the Korea Health Industry Development Institute (KHIDI) and Korea Dementia Research Center (KDRC), funded by the Ministry of Health & Welfare and Ministry of Science and ICT, Republic of Korea (HU21C0027).

AUTHOR CONTRIBUTIONS

D.L., H.C.J., E.S.K, and S.B.L. wrote the manuscript. H.C.J. and E.S.K. performed experiments. D.L., H.C.J., and E.S.K. analyzed the data. S.Y.K., J.Y.C., S.H.C., K.A.K., J.H.C., B.S.K, I.J.C., C.G.C., E.S.K., and S.B.L. provided expertise and feedback. E.S.K. and S.B.L. supervised the research.

CONFLICT OF INTEREST

The authors have no potential conflicts of interest to disclose.

ORCID

Davin Lee: https://orcid.org/0000-0002-1506-5304

Hae Chan Jeong: https://orcid.org/0009-0008-1184-2445

Seung Yeol Kim: https://orcid.org/0000-0002-9880-2495

Jin Yong Chung: https://orcid.org/0009-0009-6025-2895

Seok Hwan Cho: https://orcid.org/0009-0008-7857-9346

Kyoung Ah Kim: https://orcid.org/0009-0006-0513-9433

Jae Ho Cho: https://orcid.org/0000-0002-4037-087X

Byung Su Ko: https://orcid.org/0009-0009-1667-0985

In Jun Cha: https://orcid.org/0000-0001-7950-3804

Chang Geon Chung: https://orcid.org/0000-0001-8155-4926

Eun Seon Kim: https://orcid.org/0000-0003-4648-5296

Sung Bae Lee: https://orcid.org/0000-0002-8980-6769

FIGURE LEGENDS

Figure 1. Comparative analysis of the neurotoxicity and pathological effects of various G_4C_2 constructs in *Drosophila* models

(a) Representative images of eye phenotype in *Drosophila* models expressing denoted G_4C_2 transgenes at day 7 APE (Genotype: Control, *GMR-Gal4*/+;*UAS-luciferase*/+ | *$(G_4C_2)_{160}$*, *GMR-Gal4*/*UAS-$(G_4C_2)_{160}$*;+/+ | *$(G_4C_2)_{30}$* (III), *GMR-Gal4*/+;*UAS-$(G_4C_2)_{30}$*/+ | *$(G_4C_2)_{30}$* (II), *GMR-Gal4*/*UAS-$(G_4C_2)_{30}$*;+/+ | *$(G_4C_2)_{36}$*, *GMR-Gal4*/*UAS-$(G_4C_2)_{36}$*;+/+ | *LDS-$(G_4C_2)_{44}$*, *GMR-Gal4*/+;*UAS-LDS-$(G_4C_2)_{44}$.GR-GFP*/+ | *$(G_4C_2)_{49}$* (III), *GMR-Gal4*/+;*UAS-$(G_4C_2)_{49}$*/+ | *$(G_4C_2)_{49}$* (II), *GMR-Gal4*/*UAS-$(G_4C_2)_{49}$*;+/+) (black scale bar, 100 μm).

(b) Quantification of eye phenotype in *Drosophila* expressing denoted G_4C_2 transgenes described in Figure 1a. The degeneration score was assigned based on the criteria provided in Supplementary Figure S1b.

(c) Quantification of climbing ability in *Drosophila* expressing denoted G_4C_2 transgenes at day 3 APE (Genotype: Control, *Elav-Gal4*/+;*UAS-luciferase*/+ | *$(G_4C_2)_{160}$*, *Elav-Gal4*/*UAS-$(G_4C_2)_{160}$*;+/+ | *$(G_4C_2)_{30}$* (III), *Elav-Gal4*/+;UAS*$(G_4C_2)_{30}$*/+ | *$(G_4C_2)_{30}$* (II), *Elav-Gal4*/*UAS-$(G_4C_2)_{30}$*;+/+ | *$(G_4C_2)_{36}$*, *Elav-Gal4*/*UAS-$(G_4C_2)_{36}$*;+/+ | *LDS-$(G_4C_2)_{44}$*, *Elav-Gal4*/+;*UAS-LDS-$(G_4C_2)_{44}$.GR-GFP*/+ | *$(G_4C_2)_{49}$* (III), *Elav-Gal4*/+;*UAS-$(G_4C_2)_{49}$*/+ | *$(G_4C_2)_{49}$* (II), *Elav-Gal4*/*UAS-$(G_4C_2)_{49}$*;+/+).

(d) Quantification of climbing ability in *Drosophila* expressing denoted G_4C_2 transgenes described in Figure 1c at day 10 APE.

(e) Lifespan analysis of *Drosophila* expressing denoted G_4C_2 transgenes described in Figure 1c. Survival data were plotted using the Kaplan-Meier method. Both *$(G_4C_2)_{49}$* lines were excluded from lifespan analysis due to lethality in our experimental conditions.

Figure 2. Detection of GP DPRs in the brains of G_4C_2-expressing *Drosophila*

(a) Representative images of GP staining in the Kenyon cells of *Drosophila* brains

expressing G_4C_2 transgenes at day 10 APE. (Genotype: Control, *Elav-Gal4*/+;*UAS-luciferase*/+ | *$(G_4C_2)_{160}$*, *Elav-Gal4*/*UAS-$(G_4C_2)_{160}$*;+/+ | *$(G_4C_2)_{30}$* (III), *Elav-Gal4*/+;*UAS-$(G_4C_2)_{30}$*/+ | *$(G_4C_2)_{30}$* (II), *Elav-Gal4*/*UAS-$(G_4C_2)_{30}$*;+/+ | *$(G_4C_2)_{36}$*, *Elav-Gal4*/*UAS-$(G_4C_2)_{36}$*;+/+ | *LDS-$(G_4C_2)_{44}$*, *Elav-Gal4*/+;*UAS-LDS-$(G_4C_2)_{44}$.GR-GFP*/+) (white scale bar, 5 μm).

(b) Quantification of GP DPR staining in *Drosophila* expressing denoted G_4C_2 transgenes described in Figure 2a.

Figure 3. Evaluating drug efficacy against G_4C_2 toxicity: Impacts on lifespan, mobility, and eye degeneration in *Drosophila* models

(a) Lifespan assay on *Drosophila* expressing the G_4C_2 transgene *LDS-$(G_4C_2)_{44}$* (Genotype: *Elav-Gal4*/+;*UAS-LDS-$(G_4C_2)_{44}$.GR-GFP*/+) treated either with Control (black) or TMPyP4 at 100μM (green). Survival data were plotted using the Kaplan-Meier method.

(b) Lifespan assay on *Drosophila* expressing the G_4C_2 transgene described in Figure 3b treated either with Control (black line) or PJ34 at 5μM (red). Survival data were plotted using the Kaplan-Meier method.

(c) Quantification of climbing ability in *Drosophila* models at day 10 APE treated either with Control or TMPyP4 at 100μM. (Genotype: Control, *Elav-Gal4*/+;*UAS-luciferase*/+ | *$(G_4C_2)_{30}$* (II), *Elav-Gal4*/*UAS-$(G_4C_2)_{30}$*;+/+ | *LDS-$(G_4C_2)_{44}$*, *Elav-Gal4*/+;*UAS-LDS-$(G_4C_2)_{44}$.GR-GFP*/+)

(d) Quantification of climbing ability in *Drosophila* expressing denoted G_4C_2 transgenes described in Figure 3c at day 10 APE treated either with Control or PJ34 at 5μM.

(e) Representative images of *Drosophila* eye expressing denoted G_4C_2 transgenes at day 10 APE (Genotype: Control, *GMR-Gal4*/+;*UAS-luciferase*/+ | *$(G_4C_2)_{30}$* (II), *GMR-Gal4*/*UAS-$(G_4C_2)_{30}$*;+/+ | *LDS-$(G_4C_2)_{44}$*, *GMR-Gal4*/+;*UAS-LDS-$(G_4C_2)_{44}$.GR-GFP*/+). The flies were fed with Control (ADCW) or treated with TMPyP4 at 100μM (black scale bar, 100 μm).

(f) Quantification of eye degeneration scores in *Drosophila* expressing denoted G_4C_2 transgenes, as described in Figure 3e. fed with Control (ADCW) or treated with TMPyP4 at 100μM. Eye degeneration was scored based on the criteria provided in Supplementary Figure S1b.

(g) Representative images of *Drosophila* eye expressing denoted G_4C_2 transgenes described in Figure 3e at day 10 APE. The flies were fed with Control (DMSO 0.01%) or treated with PJ34 at 5μM.

(h) Quantification of the eye phenotype in *Drosophila* expressing denoted G_4C_2 transgenes described in Figure 3e., fed with Control (DMSO 0.01%) or treated with PJ34 at 5μM. Eye degeneration was scored based on the criteria provided in Supplementary Figure S1c.

Figure 4. Impact of representative G_4C_2-associated drugs on GP DPR in *Drosophila* models

(a) Representative images of GP staining in the Kenyon cells of *Drosophila* brains expressing G_4C_2 transgenes at day 10 APE. (Genotype: Control, *Elav-Gal4*/+;*UAS-luciferase*/+ | $(G_4C_2)_{30}$ (II), *Elav-Gal4*/*UAS-*$(G_4C_2)_{30}$;+/+ | *LDS-*$(G_4C_2)_{44}$, *Elav-Gal4*/+;*UAS-LDS-*$(G_4C_2)_{44}$*.GR-GFP*/+). The experimental lines were treated with either ACDW or TMPyP4 at 100μM (white scale bar, 5 μm).

(b) Representative images of GP staining in the Kenyon cells of *Drosophila* brains expressing G_4C_2 transgenes denoted in Figure 4a at day 10 APE. The experimental lines were treated with either DMSO (0.01%) or PJ34 at 5μM (white scale bar, 5 μm).

(c) Quantification of GP DPR staining in *Drosophila* expressing denoted G_4C_2 transgenes described in Figure 4a treated with either ACDW or TMPyP4 at 100μM.

(d) Quantification of GP DPR staining in *Drosophila* expressing denoted G_4C_2 transgenes described in Figure 4a treated with either DMSO (0.01%) or PJ34 at 5μM.

Figure 5. Summary table of the disparate phenotypic outcomes in *Drosophila* expressing $(G_4C_2)_{30}$ (II) and *LDS-*$(G_4C_2)_{44}$ treated with disease-modifying drugs

(a) The table presents the differing responses of *Drosophila* expressing $(G_4C_2)_{30}$ (II) and *LDS-*$(G_4C_2)_{44}$ when treated with three previously characterized disease modifying drugs. The symbols 'O' and 'X' are utilized to denote an ameliorating effect and no observable change respectively.

SUPPLEMENTARY MATERIALS

Supplementary Figure S1. Detailed characterization of G_4C_2 transgenes and scoring criteria for *Drosophila* eye degeneration

(a) An illustration detailing the seven publicly available G_4C_2 transgenes utilized in this study. The specific characteristics and attributes of each transgene are depicted, providing detailed explanation of their structure and potential implications in the context of our experimental design.

(b) Representative images of *Drosophila* eye and criteria for scoring *Drosophila* eye degeneration. Scores range from 1 to 5, with 1 representing control eyes showing normal phenotype and 5 indicating severe degeneration. Intermediate scores reflect increasing severity of eye degeneration characterized by ommatidia cell death, pigmentation degeneration, and eye shape deformity. A higher score represents a more severe outcome (black scale bar, 100 μm).

(c) Representative images of DMSO-fed (0.01%) *Drosophila* eye and criteria for scoring *Drosophila* eye degeneration. Scores range from 1 to 6, with 1 representing control eyes showing normal phenotype and 6 indicating severe degeneration. Intermediate scores reflect increasing severity of eye degeneration characterized by ommatidia cell death, pigmentation degeneration, and eye shape deformity. A higher score represents a more severe outcome.

Supplementary Figure S2. Detection of GR DPRs and TBPH in the brains of *LDS-$(G_4C_2)_{44}$*-expressing *Drosophila*

(a) Representative images of GR-GFP in the Kenyon cells of *Drosophila* brains expressing *LDS-$(G_4C_2)_{44}$* transgenes denoted in figure 2a at day 10 APE (white scale bar, 5 μm).

(b) Representative images of TBPH staining in the Kenyon cells of *Drosophila* brains expressing G_4C_2 described in Figure 2a (white scale bar, 1 μm). Outer and inner dashed lines indicate the borders of cell bodies and nuclei, respectively. The intensity profile of fluorescent signals representing TBPH proteins across cell bodies along red lines are presented at the bottom.

Supplementary Figure S3. Detailed experimental design and the evaluation of KPT-276 and *Rhau* expression in *Drosophila* models expressing G_4C_2 transgenes

(a) A schematic illustration of the candidate selection process, divided into three main stages: Fly Crossing, Candidate Selection, and Drug Treatment. The diagram visually represents the experimental design and subsequent selection process used to identify and test 3 potential therapeutic compounds: TMPyP4, PJ34, and KPT-276.

(b) Lifespan quantification of *Drosophila* expressing the G_4C_2 transgene described in Figure 3a. The flies were fed to either Control (black) or KPT-276 at 1μM (purple). Survival data were plotted using the Kaplan-Meier method.

(c) Climbing ability of *Drosophila* expressing G_4C_2 transgenes described in Supplementary Figure S3c at day 10 APE. The flies were subjected to either Control (black) or KPT-276 at 1μM (purple).

(d) Representative images of *Drosophila* eye expressing G_4C_2 transgenes as described in Figure 3e at day 10 APE. The flies were fed with either Control or KPT-276 at 1μM (black scale bar, 100 μm).

(e) Quantification of eye phenotype degeneration score in *Drosophila* expressing denoted G_4C_2 transgenes as described in Figure 3e. The severity of the degenerative phenotype is represented as a score based on the criteria provided in Supplementary Figure S1c.

(f) Representative images of *Drosophila* eye expressing denoted *$(G_4C_2)_{30}$* (II) transgenes at day 1 APE (Genotype: *EYFP*, *UAS-EYFP*/*UAS-$(G_4C_2)_{30}$*;*GMR-Gal4*/+ | *Rhau*, *UAS-HA-Rhau*/ *UAS-$(G_4C_2)_{30}$*;*GMR-Gal4*/+).

(g) Quantification of eye phenotype degeneration score in *Drosophila* expressing denoted *$(G_4C_2)_{30}$* (II) transgenes as described in Figure 3f. The severity of the degenerative phenotype is represented as a score based on the criteria provided in Supplementary Figure S1b.

Supplementary Figure S4. Assessment of representative G_4C_2-associated drugs on DPR expression in *Drosophila* brain cells

(a) Representative images of GP staining in the Kenyon cells of *Drosophila* brains expressing G_4C_2 transgenes denoted in Figure 4a at day 10 APE. The experimental lines were treated with either DMSO (0.01%) or KPT-276 at 1μM (white scale bar, 5 μm).

(b) Quantification of GP DPR staining in *Drosophila* expressing denoted G_4C_2 transgenes described in Figure 4a treated with either DMSO (0.01%) or KPT-276 at 1μM.

(c) Representative images of GR-GFP in the Kenyon cells of *Drosophila* brains expressing G_4C_2 transgenes denoted in figure 4a at day 10 APE. The experimental lines were treated with either ACDW or TMPyP4 at 100μM (white scale bar, 5 μm).

(d) Quantification of GR-GFP in *Drosophila* expressing denoted G_4C_2 transgenes described in Figure 4a treated with either ACDW or TMPyP4 at 100μM.

(e) Representative images of GR-GFP in the Kenyon cells of *Drosophila* brains expressing G_4C_2 transgenes denoted in figure 4a at day 10 APE. The experimental lines were treated with DMSO (0.01%), PJ34 at 5μM, or KPT-276 at 1μM (white scale bar, 5 μm).

(f) Quantification of GR-GFP in *Drosophila* expressing denoted G_4C_2 transgenes described in Figure 4a treated with DMSO (0.01%), PJ34 at 5μM, or KPT-276 at 1μM.

Supplementary Figure S5. G_4C_2 RNA quantification and assessment of toxicity through rRNA antibody staining in G_4C_2-expressing *Drosophila* lines.

(a) A table outlining the primer sets used, target locations, construct details, and resulting **Δ**Ct values for each genotype at day 10 APE. (Genotype: Control, *Elav-Gal4*/+;*UAS-luciferase*/+ | *$(G_4C_2)_{160}$*, *Elav-Gal4*/*UAS-$(G_4C_2)_{160}$*;+/+ | *$(G_4C_2)_{30}$* (III), *Elav-Gal4*/+;*UAS-$(G_4C_2)_{30}$*/+ | *$(G_4C_2)_{30}$* (II), *Elav-Gal4*/*UAS-$(G_4C_2)_{30}$*;+/+ | *LDS-$(G_4C_2)_{44}$*, *Elav-Gal4*/+;*UAS-LDS-$(G_4C_2)_{44}$.GR-GFP*/+)

(b) Quantification of $2^{-\Delta\Delta Ct}$ fold changes in *Drosophila* expressing *$(G_4C_2)_{160}$* detailed in Supplementary Figure S5a.

(c) Quantification of $2^{-\Delta\Delta Ct}$ fold changes in *Drosophila* expressing $(G_4C_2)_{30}$ (III) and $(G_4C_2)_{30}$ (II) detailed in Supplementary Figure S5a.
(d) Quantification of $2^{-\Delta\Delta Ct}$ fold changes in *Drosophila* expressing *LDS-*$(G_4C_2)_{44}$ detailed in Supplementary Figure S5a.
(e) Representative images of Kenyon cells from the specified Drosophila genotypes detailed in Supplementary Figure S5a stained with an rRNA antibody. Yellow arrowheads indicate rRNA foci (white scale bar, 2 μm).
(f) Quantification of the number of cytoplasmic rRNA foci in *Drosophila* expressing genotype detailed in Supplementary Figure S5a.

REFERENCES

Ash, P. E., Bieniek, K. F., Gendron, T. F., Caulfield, T., Lin, W. L., Dejesus-Hernandez, M., van Blitterswijk, M. M., Jansen-West, K., Paul, J. W., 3rd, Rademakers, R., Boylan, K. B., Dickson, D. W., & Petrucelli, L. (2013). Unconventional translation of C9ORF72 GGGGCC expansion generates insoluble polypeptides specific to c9FTD/ALS. *Neuron*, *77*(4), 639-646. https://doi.org/10.1016/j.neuron.2013.02.004

Batra, R., & Lee, C. W. (2017). Mouse Models of C9orf72 Hexanucleotide Repeat Expansion in Amyotrophic Lateral Sclerosis/ Frontotemporal Dementia. *Front Cell Neurosci*, *11*, 196. https://doi.org/10.3389/fncel.2017.00196

Boeynaems, S., Bogaert, E., Michiels, E., Gijselinck, I., Sieben, A., Jovicic, A., De Baets, G., Scheveneels, W., Steyaert, J., Cuijt, I., Verstrepen, K. J., Callaerts, P., Rousseau, F., Schymkowitz, J., Cruts, M., Van Broeckhoven, C., Van Damme, P., Gitler, A. D., Robberecht, W., & Van Den Bosch, L. (2016). Drosophila screen connects nuclear transport genes to DPR pathology in c9ALS/FTD. *Sci Rep*, *6*, 20877. https://doi.org/10.1038/srep20877

Boivin, M., Pfister, V., Gaucherot, A., Ruffenach, F., Negroni, L., Sellier, C., & Charlet-Berguerand, N. (2020). Reduced autophagy upon C9ORF72 loss synergizes with dipeptide repeat protein toxicity in G4C2 repeat expansion disorders. *EMBO J*, *39*(4), e100574. https://doi.org/10.15252/embj.2018100574

Byrne, S., Heverin, M., Elamin, M., Bede, P., Lynch, C., Kenna, K., MacLaughlin, R., Walsh, C., Al Chalabi, A., & Hardiman, O. (2013). Aggregation of neurologic and neuropsychiatric disease in amyotrophic lateral sclerosis kindreds: a population-based case-control cohort study of familial and sporadic amyotrophic lateral sclerosis. *Ann Neurol*, *74*(5), 699-708. https://doi.org/10.1002/ana.23969

Cho, J. H., Jo, M. G., Kim, E. S., Lee, N. Y., Kim, S. H., Chung, C. G., Park, J. H., & Lee, S. B. (2022). CBP-Mediated Acetylation of Importin alpha Mediates Calcium-Dependent Nucleocytoplasmic Transport of Selective Proteins in Drosophila Neurons. *Mol Cells*, *45*(11), 855-867. https://doi.org/10.14348/molcells.2022.0104

Chou, C. C., Zhang, Y., Umoh, M. E., Vaughan, S. W., Lorenzini, I., Liu, F., Sayegh, M., Donlin-Asp, P. G., Chen, Y. H., Duong, D. M., Seyfried, N. T., Powers, M. A., Kukar, T., Hales, C. M., Gearing,

M., Cairns, N. J., Boylan, K. B., Dickson, D. W., Rademakers, R., . . . Rossoll, W. (2018). TDP-43 pathology disrupts nuclear pore complexes and nucleocytoplasmic transport in ALS/FTD. *Nat Neurosci*, *21*(2), 228-239. https://doi.org/10.1038/s41593-017-0047-3

Chung, C. G., Kwon, M. J., Jeon, K. H., Hyeon, D. Y., Han, M. H., Park, J. H., Cha, I. J., Cho, J. H., Kim, K., Rho, S., Kim, G. R., Jeong, H., Lee, J. W., Kim, T., Kim, K., Kim, K. P., Ehlers, M. D., Hwang, D., & Lee, S. B. (2017). Golgi Outpost Synthesis Impaired by Toxic Polyglutamine Proteins Contributes to Dendritic Pathology in Neurons. *Cell Rep*, *20*(2), 356-369. https://doi.org/10.1016/j.celrep.2017.06.059

Conlon, E. G., Lu, L., Sharma, A., Yamazaki, T., Tang, T., Shneider, N. A., & Manley, J. L. (2016). The C9ORF72 GGGGCC expansion forms RNA G-quadruplex inclusions and sequesters hnRNP H to disrupt splicing in ALS brains. *Elife*, *5*. https://doi.org/10.7554/eLife.17820

Cunningham, K. M., Maulding, K., Ruan, K., Senturk, M., Grima, J. C., Sung, H., Zuo, Z., Song, H., Gao, J., Dubey, S., Rothstein, J. D., Zhang, K., Bellen, H. J., & Lloyd, T. E. (2020). TFEB/Mitf links impaired nuclear import to autophagolysosomal dysfunction in C9-ALS. *Elife*, *9*. https://doi.org/10.7554/eLife.59419

Dafinca, R., Scaber, J., Ababneh, N., Lalic, T., Weir, G., Christian, H., Vowles, J., Douglas, A. G., Fletcher-Jones, A., Browne, C., Nakanishi, M., Turner, M. R., Wade-Martins, R., Cowley, S. A., & Talbot, K. (2016). C9orf72 Hexanucleotide Expansions Are Associated with Altered Endoplasmic Reticulum Calcium Homeostasis and Stress Granule Formation in Induced Pluripotent Stem Cell-Derived Neurons from Patients with Amyotrophic Lateral Sclerosis and Frontotemporal Dementia. *Stem Cells*, *34*(8), 2063-2078. https://doi.org/10.1002/stem.2388

DeJesus-Hernandez, M., Mackenzie, I. R., Boeve, B. F., Boxer, A. L., Baker, M., Rutherford, N. J., Nicholson, A. M., Finch, N. A., Flynn, H., Adamson, J., Kouri, N., Wojtas, A., Sengdy, P., Hsiung, G. Y., Karydas, A., Seeley, W. W., Josephs, K. A., Coppola, G., Geschwind, D. H., . . . Rademakers, R. (2011). Expanded GGGGCC hexanucleotide repeat in noncoding region of C9ORF72 causes chromosome 9p-linked FTD and ALS. *Neuron*, *72*(2), 245-256. https://doi.org/10.1016/j.neuron.2011.09.011

Devenney, E., Hornberger, M., Irish, M., Mioshi, E., Burrell, J., Tan, R., Kiernan, M. C., & Hodges, J. R. (2014). Frontotemporal dementia associated with the C9ORF72 mutation: a unique clinical profile. *JAMA Neurol*, *71*(3), 331-339. https://doi.org/10.1001/jamaneurol.2013.6002

Dubey, S. K., Maulding, K., Sung, H., & Lloyd, T. E. (2022). Nucleoporins are degraded via upregulation of ESCRT-III/Vps4 complex in Drosophila models of C9-ALS/FTD. *Cell Rep*, *40*(12), 111379. https://doi.org/10.1016/j.celrep.2022.111379

Gao, J., Mewborne, Q. T., Girdhar, A., Sheth, U., Coyne, A. N., Punathil, R., Kang, B. G., Dasovich, M., Veire, A., DeJesus Hernandez, M., Liu, S., Shi, Z., Dafinca, R., Fouquerel, E., Talbot, K., Kam, T. I., Zhang, Y. J., Dickson, D., Petrucelli, L., . . . Zhang, K. (2022). Poly(ADP-ribose) promotes toxicity of C9ORF72 arginine-rich dipeptide repeat proteins. *Sci Transl Med*, *14*(662), eabq3215. https://doi.org/10.1126/scitranslmed.abq3215

Gasset-Rosa, F., Lu, S., Yu, H., Chen, C., Melamed, Z., Guo, L., Shorter, J., Da Cruz, S., & Cleveland, D.

W. (2019). Cytoplasmic TDP-43 De-mixing Independent of Stress Granules Drives Inhibition of Nuclear Import, Loss of Nuclear TDP-43, and Cell Death. *Neuron*, *102*(2), 339-357 e337. https://doi.org/10.1016/j.neuron.2019.02.038

Goodman, L. D., Prudencio, M., Kramer, N. J., Martinez-Ramirez, L. F., Srinivasan, A. R., Lan, M., Parisi, M. J., Zhu, Y., Chew, J., Cook, C. N., Berson, A., Gitler, A. D., Petrucelli, L., & Bonini, N. M. (2019). Toxic expanded GGGGCC repeat transcription is mediated by the PAF1 complex in C9orf72-associated FTD. *Nat Neurosci*, *22*(6), 863-874. https://doi.org/10.1038/s41593-019-0396-1

Goodman, L. D., Prudencio, M., Srinivasan, A. R., Rifai, O. M., Lee, V. M., Petrucelli, L., & Bonini, N. M. (2019). eIF4B and eIF4H mediate GR production from expanded G4C2 in a Drosophila model for C9orf72-associated ALS. *Acta Neuropathol Commun*, *7*(1), 62. https://doi.org/10.1186/s40478-019-0711-9

Haeusler, A. R., Donnelly, C. J., & Rothstein, J. D. (2016). The expanding biology of the C9orf72 nucleotide repeat expansion in neurodegenerative disease. *Nat Rev Neurosci*, *17*(6), 383-395. https://doi.org/10.1038/nrn.2016.38

Kearse, M. G., Green, K. M., Krans, A., Rodriguez, C. M., Linsalata, A. E., Goldstrohm, A. C., & Todd, P. K. (2016). CGG Repeat-Associated Non-AUG Translation Utilizes a Cap-Dependent Scanning Mechanism of Initiation to Produce Toxic Proteins. *Mol Cell*, *62*(2), 314-322. https://doi.org/10.1016/j.molcel.2016.02.034

Kim, E. S., Chung, C. G., Park, J. H., Ko, B. S., Park, S. S., Kim, Y. H., Cha, I. J., Kim, J., Ha, C. M., Kim, H. J., & Lee, S. B. (2021). C9orf72-associated arginine-rich dipeptide repeats induce RNA-dependent nuclear accumulation of Staufen in neurons. *Hum Mol Genet*, *30*(12), 1084-1100. https://doi.org/10.1093/hmg/ddab089

Kramer, N. J., Carlomagno, Y., Zhang, Y. J., Almeida, S., Cook, C. N., Gendron, T. F., Prudencio, M., Van Blitterswijk, M., Belzil, V., Couthouis, J., Paul, J. W., 3rd, Goodman, L. D., Daughrity, L., Chew, J., Garrett, A., Pregent, L., Jansen-West, K., Tabassian, L. J., Rademakers, R., . . . Gitler, A. D. (2016). Spt4 selectively regulates the expression of C9orf72 sense and antisense mutant transcripts. *Science*, *353*(6300), 708-712. https://doi.org/10.1126/science.aaf7791

Kwiatkowski, T. J., Jr., Bosco, D. A., Leclerc, A. L., Tamrazian, E., Vanderburg, C. R., Russ, C., Davis, A., Gilchrist, J., Kasarskis, E. J., Munsat, T., Valdmanis, P., Rouleau, G. A., Hosler, B. A., Cortelli, P., de Jong, P. J., Yoshinaga, Y., Haines, J. L., Pericak-Vance, M. A., Yan, J., . . . Brown, R. H., Jr. (2009). Mutations in the FUS/TLS gene on chromosome 16 cause familial amyotrophic lateral sclerosis. *Science*, *323*(5918), 1205-1208. https://doi.org/10.1126/science.1166066

Lee, J., Song, X., Hyun, B., Jeon, C. O., & Hyun, S. (2023). Drosophila Gut Immune Pathway Suppresses Host Development-Promoting Effects of Acetic Acid Bacteria. *Mol Cells*, *46*(10), 637-653. https://doi.org/10.14348/molcells.2023.0141

Lee, K. H., Zhang, P., Kim, H. J., Mitrea, D. M., Sarkar, M., Freibaum, B. D., Cika, J., Coughlin, M., Messing, J., Molliex, A., Maxwell, B. A., Kim, N. C., Temirov, J., Moore, J., Kolaitis, R. M., Shaw, T. I., Bai, B., Peng, J., Kriwacki, R. W., & Taylor, J. P. (2016). C9orf72 Dipeptide Repeats Impair the

Assembly, Dynamics, and Function of Membrane-Less Organelles. *Cell*, *167*(3), 774-788 e717. https://doi.org/10.1016/j.cell.2016.10.002

Lee, Y., Kim, J., Kim, H., Han, J. E., Kim, S., Kang, K. H., Kim, D., Kim, J. M., & Koh, H. (2022). Pyruvate Dehydrogenase Kinase Protects Dopaminergic Neurons from Oxidative Stress in Drosophila DJ-1 Null Mutants. *Mol Cells*, *45*(7), 454-464. https://doi.org/10.14348/molcells.2022.5002

Lee, Y. B., Chen, H. J., Peres, J. N., Gomez-Deza, J., Attig, J., Stalekar, M., Troakes, C., Nishimura, A. L., Scotter, E. L., Vance, C., Adachi, Y., Sardone, V., Miller, J. W., Smith, B. N., Gallo, J. M., Ule, J., Hirth, F., Rogelj, B., Houart, C., & Shaw, C. E. (2013). Hexanucleotide repeats in ALS/FTD form length-dependent RNA foci, sequester RNA binding proteins, and are neurotoxic. *Cell Rep*, *5*(5), 1178-1186. https://doi.org/10.1016/j.celrep.2013.10.049

Li, C., Wu, B., Chen, S., Hao, K., Yang, J., Cao, H., Yang, S., Wu, Z. S., & Shen, Z. (2021). Structural requirement of G-quadruplex/aptamer-combined DNA macromolecule serving as efficient drug carrier for cancer-targeted drug delivery. *Eur J Pharm Biopharm*, *159*, 221-227. https://doi.org/10.1016/j.ejpb.2020.11.021

Lin, M. J., Cheng, C. W., & Shen, C. K. (2011). Neuronal function and dysfunction of Drosophila dTDP. *PLoS One*, *6*(6), e20371. https://doi.org/10.1371/journal.pone.0020371

Liu, H., Lu, Y. N., Paul, T., Periz, G., Banco, M. T., Ferre-D'Amare, A. R., Rothstein, J. D., Hayes, L. R., Myong, S., & Wang, J. (2021). A Helicase Unwinds Hexanucleotide Repeat RNA G-Quadruplexes and Facilitates Repeat-Associated Non-AUG Translation. *J Am Chem Soc*, *143*(19), 7368-7379. https://doi.org/10.1021/jacs.1c00131

Majounie, E., Renton, A. E., Mok, K., Dopper, E. G., Waite, A., Rollinson, S., Chio, A., Restagno, G., Nicolaou, N., Simon-Sanchez, J., van Swieten, J. C., Abramzon, Y., Johnson, J. O., Sendtner, M., Pamphlett, R., Orrell, R. W., Mead, S., Sidle, K. C., Houlden, H., . . . Traynor, B. J. (2012). Frequency of the C9orf72 hexanucleotide repeat expansion in patients with amyotrophic lateral sclerosis and frontotemporal dementia: a cross-sectional study. *Lancet Neurol*, *11*(4), 323-330. https://doi.org/10.1016/S1474-4422(12)70043-1

McEachin, Z. T., Parameswaran, J., Raj, N., Bassell, G. J., & Jiang, J. (2020). RNA-mediated toxicity in C9orf72 ALS and FTD. *Neurobiol Dis*, *145*, 105055. https://doi.org/10.1016/j.nbd.2020.105055

Mishra, S. K., Shankar, U., Jain, N., Sikri, K., Tyagi, J. S., Sharma, T. K., Mergny, J. L., & Kumar, A. (2019). Characterization of G-Quadruplex Motifs in espB, espK, and cyp51 Genes of Mycobacterium tuberculosis as Potential Drug Targets. *Mol Ther Nucleic Acids*, *16*, 698-706. https://doi.org/10.1016/j.omtn.2019.04.022

Mizielinska, S., Gronke, S., Niccoli, T., Ridler, C. E., Clayton, E. L., Devoy, A., Moens, T., Norona, F. E., Woollacott, I. O. C., Pietrzyk, J., Cleverley, K., Nicoll, A. J., Pickering-Brown, S., Dols, J., Cabecinha, M., Hendrich, O., Fratta, P., Fisher, E. M. C., Partridge, L., & Isaacs, A. M. (2014). C9orf72 repeat expansions cause neurodegeneration in Drosophila through arginine-rich proteins. *Science*, *345*(6201), 1192-1194. https://doi.org/10.1126/science.1256800

Park, J. H., Chung, C. G., Park, S. S., Lee, D., Kim, K. M., Jeong, Y., Kim, E. S., Cho, J. H., Jeon, Y. M., Shen, C. J., Kim, H. J., Hwang, D., & Lee, S. B. (2020). Cytosolic calcium regulates cytoplasmic

accumulation of TDP-43 through Calpain-A and Importin alpha3. *Elife*, *9*. https://doi.org/10.7554/eLife.60132

Pradhan, R. N., Shrestha, B., & Lee, Y. (2023). Molecular Basis of Hexanoic Acid Taste in Drosophila melanogaster. *Mol Cells*, *46*(7), 451-460. https://doi.org/10.14348/molcells.2023.0035

Rosen, D. R., Siddique, T., Patterson, D., Figlewicz, D. A., Sapp, P., Hentati, A., Donaldson, D., Goto, J., O'Regan, J. P., Deng, H. X., & et al. (1993). Mutations in Cu/Zn superoxide dismutase gene are associated with familial amyotrophic lateral sclerosis. *Nature*, *362*(6415), 59-62. https://doi.org/10.1038/362059a0

Ryu, T. H., Subramanian, M., Yeom, E., & Yu, K. (2022). The prominin-like Gene Expressed in a Subset of Dopaminergic Neurons Regulates Locomotion in Drosophila. *Mol Cells*, *45*(9), 640-648. https://doi.org/10.14348/molcells.2022.0006

Schmidt, J., Braggio, E., Kortuem, K. M., Egan, J. B., Zhu, Y. X., Xin, C. S., Tiedemann, R. E., Palmer, S. E., Garbitt, V. M., McCauley, D., Kauffman, M., Shacham, S., Chesi, M., Bergsagel, P. L., & Stewart, A. K. (2013). Genome-wide studies in multiple myeloma identify XPO1/CRM1 as a critical target validated using the selective nuclear export inhibitor KPT-276. *Leukemia*, *27*(12), 2357-2365. https://doi.org/10.1038/leu.2013.172

Shatunov, A., Mok, K., Newhouse, S., Weale, M. E., Smith, B., Vance, C., Johnson, L., Veldink, J. H., van Es, M. A., van den Berg, L. H., Robberecht, W., Van Damme, P., Hardiman, O., Farmer, A. E., Lewis, C. M., Butler, A. W., Abel, O., Andersen, P. M., Fogh, I., . . . Al-Chalabi, A. (2010). Chromosome 9p21 in sporadic amyotrophic lateral sclerosis in the UK and seven other countries: a genome-wide association study. *Lancet Neurol*, *9*(10), 986-994. https://doi.org/10.1016/S1474-4422(10)70197-6

Shi, Y., Lin, S., Staats, K. A., Li, Y., Chang, W. H., Hung, S. T., Hendricks, E., Linares, G. R., Wang, Y., Son, E. Y., Wen, X., Kisler, K., Wilkinson, B., Menendez, L., Sugawara, T., Woolwine, P., Huang, M., Cowan, M. J., Ge, B., . . . Ichida, J. K. (2018). Haploinsufficiency leads to neurodegeneration in C9ORF72 ALS/FTD human induced motor neurons. *Nat Med*, *24*(3), 313-325. https://doi.org/10.1038/nm.4490

Solomon, D. A., Stepto, A., Au, W. H., Adachi, Y., Diaper, D. C., Hall, R., Rekhi, A., Boudi, A., Tziortzouda, P., Lee, Y. B., Smith, B., Bridi, J. C., Spinelli, G., Dearlove, J., Humphrey, D. M., Gallo, J. M., Troakes, C., Fanto, M., Soller, M., . . . Hirth, F. (2018). A feedback loop between dipeptide-repeat protein, TDP-43 and karyopherin-alpha mediates C9orf72-related neurodegeneration. *Brain*, *141*(10), 2908-2924. https://doi.org/10.1093/brain/awy241

Tran, H., Almeida, S., Moore, J., Gendron, T. F., Chalasani, U., Lu, Y., Du, X., Nickerson, J. A., Petrucelli, L., Weng, Z., & Gao, F. B. (2015). Differential Toxicity of Nuclear RNA Foci versus Dipeptide Repeat Proteins in a Drosophila Model of C9ORF72 FTD/ALS. *Neuron*, *87*(6), 1207-1214. https://doi.org/10.1016/j.neuron.2015.09.015

Tseng, Y. J., Sandwith, S. N., Green, K. M., Chambers, A. E., Krans, A., Raimer, H. M., Sharlow, M. E., Reisinger, M. A., Richardson, A. E., Routh, E. D., Smaldino, M. A., Wang, Y. H., Vaughn, J. P., Todd, P. K., & Smaldino, P. J. (2021). The RNA helicase DHX36-G4R1 modulates C9orf72

GGGGCC hexanucleotide repeat-associated translation. *J Biol Chem*, *297*(2), 100914. https://doi.org/10.1016/j.jbc.2021.100914

Van Daele, S. H., Moisse, M., van Vugt, J., Zwamborn, R. A. J., van der Spek, R., van Rheenen, W., Van Eijk, K., Kenna, K., Corcia, P., Vourc'h, P., Couratier, P., Hardiman, O., McLaughin, R., Gotkine, M., Drory, V., Ticozzi, N., Silani, V., Ratti, A., de Carvalho, M., . . . Van Damme, P. (2023). Genetic variability in sporadic amyotrophic lateral sclerosis. *Brain*. https://doi.org/10.1093/brain/awad120

Vanneste, J., & Van Den Bosch, L. (2021). The Role of Nucleocytoplasmic Transport Defects in Amyotrophic Lateral Sclerosis. *Int J Mol Sci*, *22*(22). https://doi.org/10.3390/ijms222212175

Wang, Z. F., Ursu, A., Childs-Disney, J. L., Guertler, R., Yang, W. Y., Bernat, V., Rzuczek, S. G., Fuerst, R., Zhang, Y. J., Gendron, T. F., Yildirim, I., Dwyer, B. G., Rice, J. E., Petrucelli, L., & Disney, M. D. (2019). The Hairpin Form of r(G(4)C(2))(exp) in c9ALS/FTD Is Repeat-Associated Non-ATG Translated and a Target for Bioactive Small Molecules. *Cell Chem Biol*, *26*(2), 179-190 e112. https://doi.org/10.1016/j.chembiol.2018.10.018

Wen, X., An, P., Li, H., Zhou, Z., Sun, Y., Wang, J., Ma, L., & Lu, B. (2020). Tau Accumulation via Reduced Autophagy Mediates GGGGCC Repeat Expansion-Induced Neurodegeneration in Drosophila Model of ALS. *Neurosci Bull*, *36*(12), 1414-1428. https://doi.org/10.1007/s12264-020-00518-2

Wen, X., Tan, W., Westergard, T., Krishnamurthy, K., Markandaiah, S. S., Shi, Y., Lin, S., Shneider, N. A., Monaghan, J., Pandey, U. B., Pasinelli, P., Ichida, J. K., & Trotti, D. (2014). Antisense proline-arginine RAN dipeptides linked to C9ORF72-ALS/FTD form toxic nuclear aggregates that initiate in vitro and in vivo neuronal death. *Neuron*, *84*(6), 1213-1225. https://doi.org/10.1016/j.neuron.2014.12.010

Xu, Z., Poidevin, M., Li, X., Li, Y., Shu, L., Nelson, D. L., Li, H., Hales, C. M., Gearing, M., Wingo, T. S., & Jin, P. (2013). Expanded GGGGCC repeat RNA associated with amyotrophic lateral sclerosis and frontotemporal dementia causes neurodegeneration. *Proc Natl Acad Sci U S A*, *110*(19), 7778-7783. https://doi.org/10.1073/pnas.1219643110

Yuva-Aydemir, Y., Almeida, S., Krishnan, G., Gendron, T. F., & Gao, F. B. (2019). Transcription elongation factor AFF2/FMR2 regulates expression of expanded GGGGCC repeat-containing C9ORF72 allele in ALS/FTD. *Nat Commun*, *10*(1), 5466. https://doi.org/10.1038/s41467-019-13477-8

Zamiri, B., Reddy, K., Macgregor, R. B., Jr., & Pearson, C. E. (2014). TMPyP4 porphyrin distorts RNA G-quadruplex structures of the disease-associated r(GGGGCC)n repeat of the C9orf72 gene and blocks interaction of RNA-binding proteins. *J Biol Chem*, *289*(8), 4653-4659. https://doi.org/10.1074/jbc.C113.502336

Zhang, K., Donnelly, C. J., Haeusler, A. R., Grima, J. C., Machamer, J. B., Steinwald, P., Daley, E. L., Miller, S. J., Cunningham, K. M., Vidensky, S., Gupta, S., Thomas, M. A., Hong, I., Chiu, S. L., Huganir, R. L., Ostrow, L. W., Matunis, M. J., Wang, J., Sattler, R., . . . Rothstein, J. D. (2015). The C9orf72 repeat expansion disrupts nucleocytoplasmic transport. *Nature*, *525*(7567), 56-61. https://doi.org/10.1038/nature14973

Zu, T., Liu, Y., Banez-Coronel, M., Reid, T., Pletnikova, O., Lewis, J., Miller, T. M., Harms, M. B., Falchook, A. E., Subramony, S. H., Ostrow, L. W., Rothstein, J. D., Troncoso, J. C., & Ranum, L. P. (2013). RAN proteins and RNA foci from antisense transcripts in C9ORF72 ALS and frontotemporal dementia. *Proc Natl Acad Sci U S A*, *110*(51), E4968-4977. https://doi.org/10.1073/pnas.1315438110

Fig 1

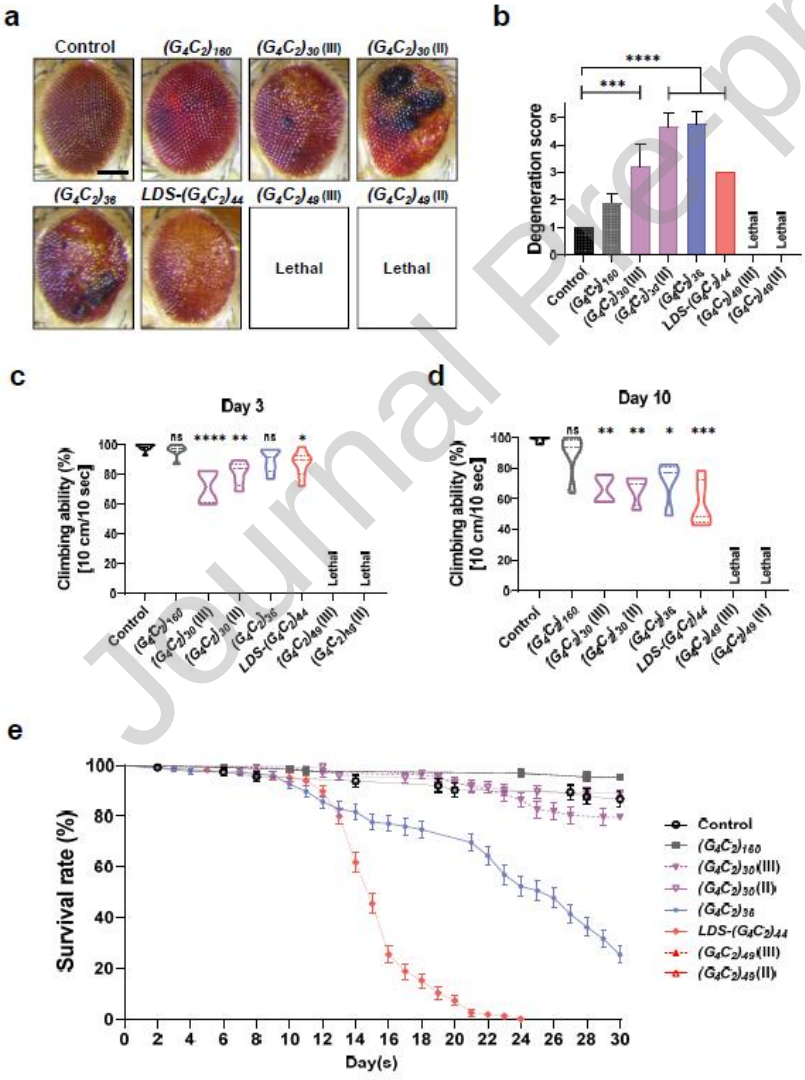

Fig 2

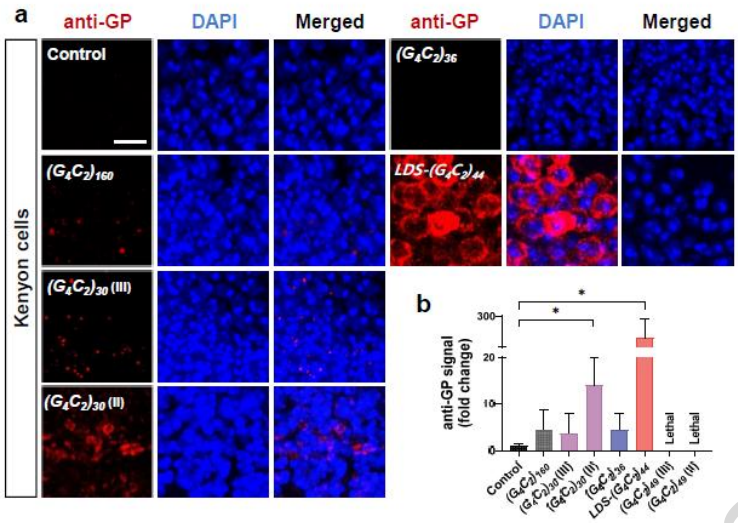

Fig 3

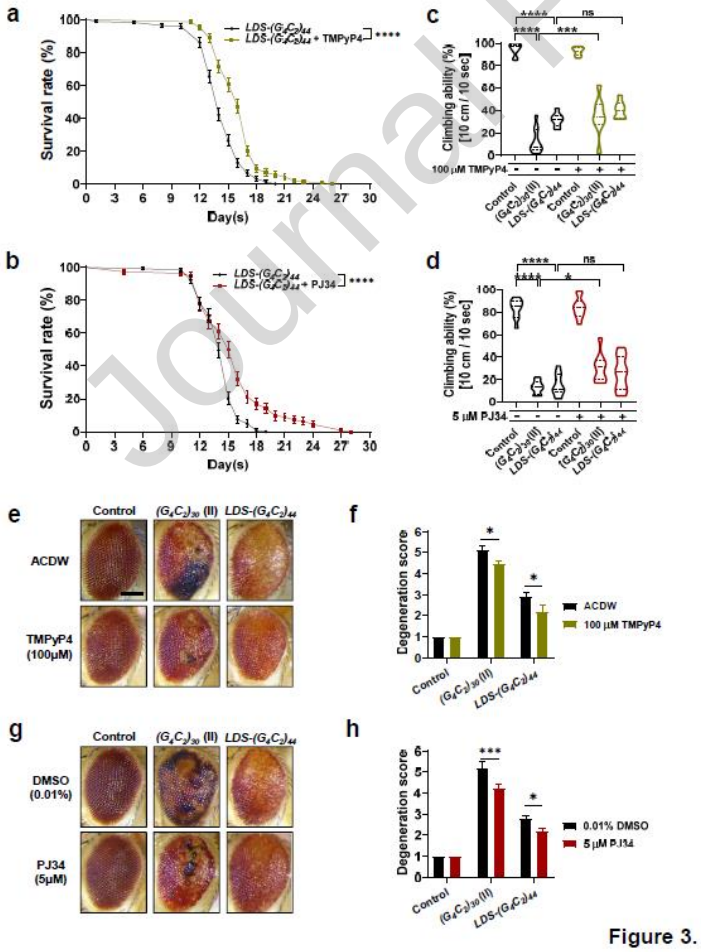

Figure 3.

Fig 4

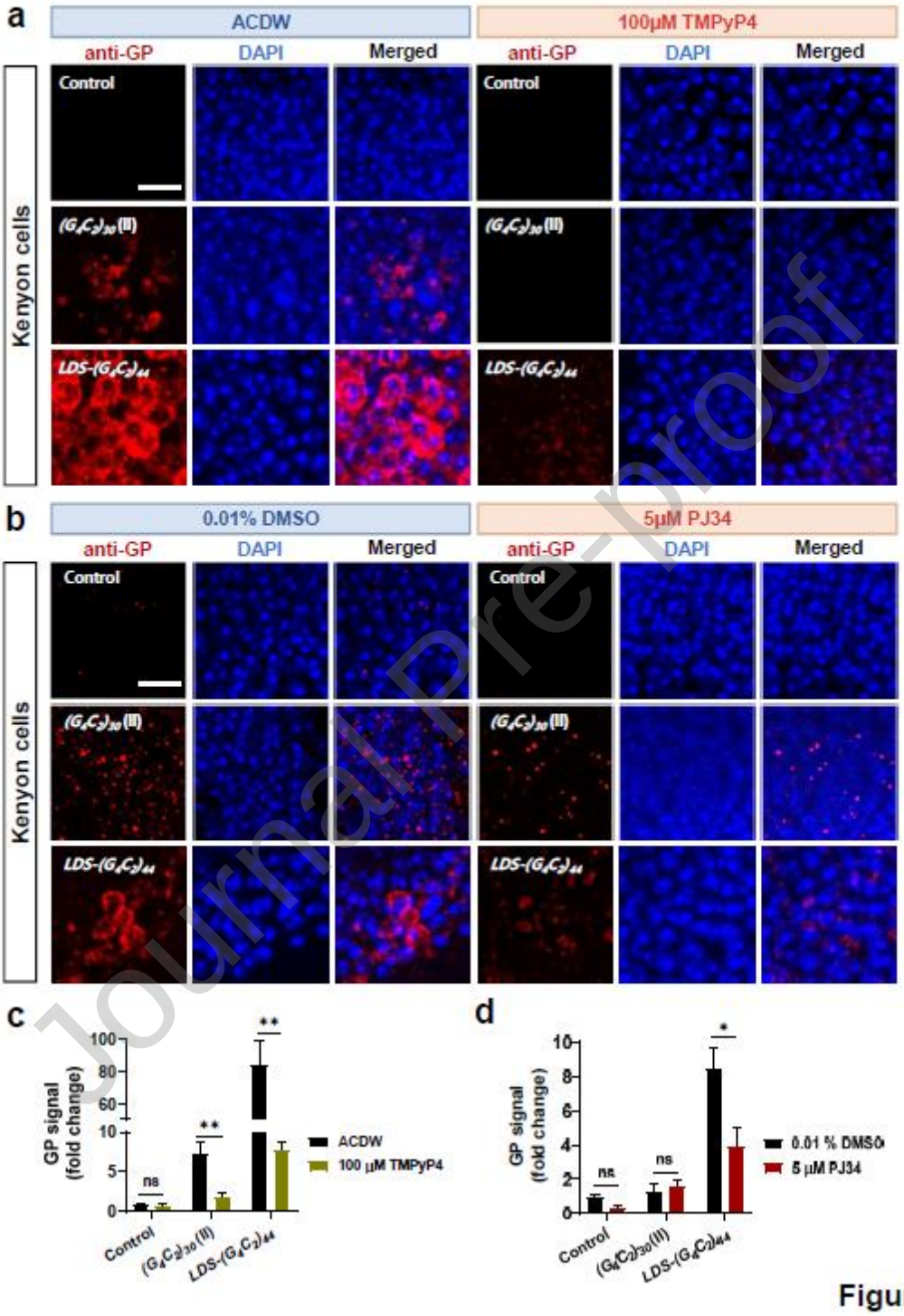

Figure 4.

Fig 5

Reference drugs		TMPyP4		PJ34		KPT-276	
G_4C_2 repeats models		$(G_4C_2)_{30}$(II)	LDS-$(G_4C_2)_{44}$	$(G_4C_2)_{30}$(II)	LDS-$(G_4C_2)_{44}$	$(G_4C_2)_{30}$(II)	LDS-$(G_4C_2)_{44}$
Pathological Outcomes	Eye Degeneration	o	o	o	o	o	x
	Lifespan	*N/A*	o	*N/A*	o	*N/A*	x
	Climbing assay (d3)	o	o	o	x	x	x
	Climbing assay (d10)	o	o	o	x	x	x
Quantity of GP signal		Decrease	Decrease	x	Decrease	x	x
Quantity of GR-GFP signal		*N/A*	x	*N/A*	x	*N/A*	x